Liquid Crystals
Publication details, including instructions for authors and subscription information:
http://www.informaworld.com/smpp/title~content=t713926090

Optical, resonant X-ray scattering, and calorimetric investigations of two liquid crystal compounds exhibiting the SmA-SmC$_\alpha$*-SmC* transitions

C. C. Huang Corresponding author[a]; Z. Q. Liu[a]; A. Cady[a]; R. Pindak[b]; W. Caliebe[b]; P. Barois[c]; H. T. Nguyen[c]; K. Ema[d]; K. Takekoshi[d]; H. Yao[d]
[a] School of Physics and Astronomy, University of Minnesota, Minneapolis, Minnesota 55455, USA [b] NSLS, Brookhaven National Laboratory, Upton, New York 11973, USA [c] Centre de Recherche Paul Pascal, CNRS, F-33600 Pessac, France [d] Department of Physics, Graduate School of Science and Engineering, Tokyo Institute of Technology, Tokyo 152, Japan

Online publication date: 19 May 2010

To cite this Article Huang Corresponding author, C. C. , Liu, Z. Q. , Cady, A. , Pindak, R. , Caliebe, W. , Barois, P. , Nguyen, H. T. , Ema, K. , Takekoshi, K. and Yao, H.(2004) 'Optical, resonant X-ray scattering, and calorimetric investigations of two liquid crystal compounds exhibiting the SmA-SmC$_\alpha$*-SmC* transitions', Liquid Crystals, 31: 1, 127 — 135
To link to this Article: DOI: 10.1080/02678290410001637167
URL: http://dx.doi.org/10.1080/02678290410001637167

LIQUID CRYSTALS, VOL. 31, NO. 1, JANUARY 2004, 127–135

Optical, resonant X-ray scattering, and calorimetric investigations of two liquid crystal compounds exhibiting the SmA-SmC$_\alpha$*-SmC* transitions

C. C. HUANG*, Z. Q. LIU, A. CADY
School of Physics and Astronomy, University of Minnesota, Minneapolis, Minnesota 55455, USA

R. PINDAK, W. CALIEBE
NSLS, Brookhaven National Laboratory, Upton, New York 11973, USA

P. BAROIS, H. T. NGUYEN
Centre de Recherche Paul Pascal, CNRS, Universite Bordeaux 1, Avenue A. Schweitzer, F-33600 Pessac, France

K. EMA, K. TAKEKOSHI and H. YAO
Department of Physics, Graduate School of Science and Engineering, Tokyo Institute of Technology, 2-12-1 Oh-okayama, Meguro, Tokyo 152, Japan

(*Received 2 September 2003; accepted 15 September 2003*)

Three experimental measurements have been conducted to investigate the nature of the SmA–SmC$_\alpha$*–SmC* phase transitions of two liquid crystal compounds. The SmA-SmC$_\alpha$* transition shows a continuous transition with *XY*-like critical exponents. The SmC$_\alpha$*-SmC* transition displays a rapid variation of the incommensurate helical pitch. One of the compounds shows a small jump in the helical pitch, which signals a first order transition and is consistent with high resolution calorimetric results.

1. Introduction

Soon after the discovery of the SmC$_A$* phase in a liquid crystal compound exhibiting large spontaneous polarization [1], three intermediate SmC* variant phases, namely SmC$_\alpha$*, SmC$_{F12}$*, and SmC$_{F11}$* were identified by differential scanning calorimetry and electro-optical studies [2, 3]. During cooling, the complete transition sequence below the SmA phase is SmC$_\alpha$*–SmC*–SmC$_{F12}$*–SmC$_{F11}$*–SmC$_A$*. In similarity to the SmA phase, all five SmC* variant phases possess liquid-like positional order within each smectic layer, while the molecules within each layer have an average tilt angle with respect to the layer normal. Conventional X-ray scattering results indicate that the bulk tilt angle is spatially homogeneous in all SmC* variant phases and varies with temperature [4]. Consequently, the SmC* variant phases are distinguished by how the tilt-azimuthal angle varies between layers. Beyond the potential technological benefits of high polarization liquid crystal phases for applications involving fast electro-optical switching devices [5], there are two primary motivations to study the SmC* variant phases. First, it is important to determine their interlayer orientational order. Second, we would like to understand the molecular interactions that produce this nano-scale orientational order.

Numerous experimental probes have been employed to determine the molecular orientational arrangements in the three new intermediate SmC* variant phases [6]. Thus far, the most direct structural information has been acquired by polarization-analysed resonant X-ray diffraction (RXD) from thick free-standing films (FSFs) of several liquid crystal compounds that have at least one heavy element (S, Se, or Cl) in the core of the molecule [7–9].

The RXD from 10OTBBB1M7 (for structure see figure 1) provided the first unambiguous demonstration that the SmC$_\alpha$* phase possesses an incommensurate

*Author for correspondence; e-mail: huang001@umn.edu

Liquid Crystals ISSN 0267-8292 print/ISSN 1366-5855 online © 2004 Taylor & Francis Ltd
http://www.tandf.co.uk/journals
DOI: 10.1080/02678290410001637167

a) 11OHFBBB1M7

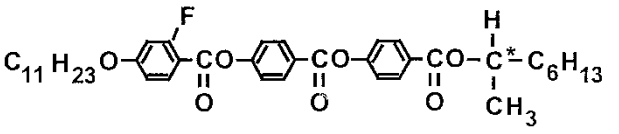

Isotropic (120) SmA (94) SmC_α* (91) SmC*

b) 11OTBBB1M7

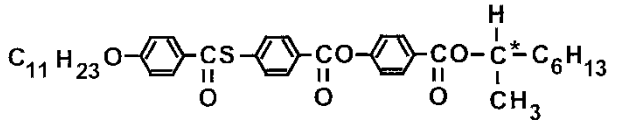

Isotropic (149) SmA (127) SmC_α* (125) SmC*

Figure 1. Molecular structures and relevant transition sequences for compounds (*a*) 11OHFBBB1M7 and (*b*) 11OTBBB1M7. All temperatures are in °C.

nano-scale helical pitch (INHP) [7]. On cooling, the INHP decreases from about 8 to 5 layers within the SmC_α* temperature range [8]; the layer thickness is about 3.5 nm. Subsequent optical studies of three liquid crystal compounds confirmed similar temperature variations of INHP in the SmC_α* phase [10–12]. Meanwhile, experimental results from other liquid crystal compounds have revealed a very different temperature variation of INHP [12–14]. On cooling these compounds, the INHP found in the SmC_α* phase (about 10 layers) increases to the longer helical pitch (about 100 layers) found in the SmC* phase, with or without a jump at the transition temperature. Common to all the SmC* variant phases, chirality is an important symmetry-breaking mechanism that gives rise to spontaneous polarization within the layers. Although chirality is an important contributor to molecular orientational order, to the best of our knowledge, it is too weak an effect to cause the INHP structure.

To date, numerous theoretical models have been proposed to explain the stability of these SmC* variant phases [15–21]. Among them, the phenomenological model proposed by Olson *et al.* [21], offers a remarkable physical insight into the stability of these five SmC* variant phases. Several theoretical models suggest that the INHP found in the SmC_α* phase is caused by the frustration between the nearest-neighbor layer (n.n.) ferroelectric-like coupling and the next-nearest-neighbor layer (n.n.n.) antiferroelectric-like interaction. Thus, in contrast to the optical helical pitch found in the conventional SmC* phase, which is $\sim 1\,\mu m$ and due to the molecular chirality, it is the short range interlayer interactions that produce the INHP in the SmC_α* phase. Moreover, the transition from SmC_α* to SmC* can be characterized by the temperature evolution of the incommensurate helical pitch. Thus, there is no symmetry change through such a transition, which is then equivalent to the well known liquid–gas transition. In general, the transition should be first order, terminate at a critical point, and then undergo a continuous evolution upon variation of one of the physical parameters, e.g. the concentration of a binary mixture.

To gain more physical insight into the nature of the SmA–SmC_α*–SmC* transitions, we have investigated them using three experimental methods: resonant x-ray diffraction, differential optical reflectivity and calorimetry. Two liquid crystal compounds, 11OTBBB1M7 and 11OHFBBB1M7 were mainly used for our studies. Their molecular structures and phase sequences are given in figure 1. In the RXD studies, we used 11OTBBB1M7, which has a sulphur atom in the core of the molecule. In the optical reflectivity studies, 11OHFBBB1M7 was used. Heat capacity measurements were conducted on both compounds. The SmA–SmC_α* transition is found to be continuous, while the SmC_α*–SmC* transition is weakly first order.

2. Resonant X-ray diffraction studies

Our research group has demonstrated that polarization analysed RXD is the most powerful experimental probe for determining the molecular nano-scale orientational order in liquid crystalline phases [7–9]. For this experimental work, we used beamline X19A at the National Synchrotron Light Source, Brookhaven National Laboratory. To begin the study we measured the sulphur fluorescence of a powder sample of 11OTBBB1M7 whilst scanning the incident X-ray energy. Afterward, the incident X-ray energy was set to the peak of the fluorescence spectrum at 2473 eV (namely, the resonant energy) near the sulphur K-edge. A thick FSF of more than 500 layers was prepared inside a temperature-regulated oven. Although short at this energy, the penetration length of X-rays is at least equal to (or larger than) the thickness of the FSF. The contribution of the few interface-distorted surface layers to the scattering is therefore negligible. From the (0 0 1) Bragg peak position obtained at 129.21°C in the SmA phase, the layer spacing was measured to be 39.61 Å.

To determine the temperature variation of the helical pitch, we performed RXD near the (0 0 2) Bragg peak. The data from one such experimental run is shown in figure 2. The sample was in the SmC* phase at 120.13°C. The solid dots are data obtained while the incident X-ray energy was tuned to the resonant energy. Both $m = +1$, and -1 satellite peaks at Q_+/Q_o and Q_-/Q_o are visible. The data acquired on increasing the

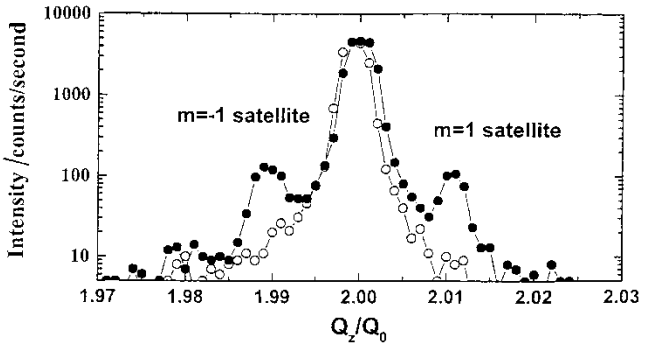

Figure 2. A Q_z scan through the (0 0 2) peak of a thick 11OTBBB1M7 FSF at E_o (solid dots) and at E_o+20 eV (open circles); E_o is the resonant energy. The sample was in the SmC* phase at 120.13°C. Both $m=\pm1$ satellite peaks are visible.

incident X-ray energy by 20 eV are shown as open circles; the satellite peaks disappear. At each temperature, the pitch is equal to $Q_o/[(Q_+-Q_-)/2]$. Figure 3 displays the temperature evolution of the short helical pitch of 11OTBBB1M7 through the SmC_α*–SmC* transition obtained from several experimental runs on two different films. Below 123°C, the magnitude of the helical pitch is about 95 layers. On heating, between 123 and 125°C the pitch rapidly decreases. Above 126°C the size of the INHP is less than 15 layers. A small jump in the helical pitch around 124.6°C was detected; this indicates the transition to be first order,

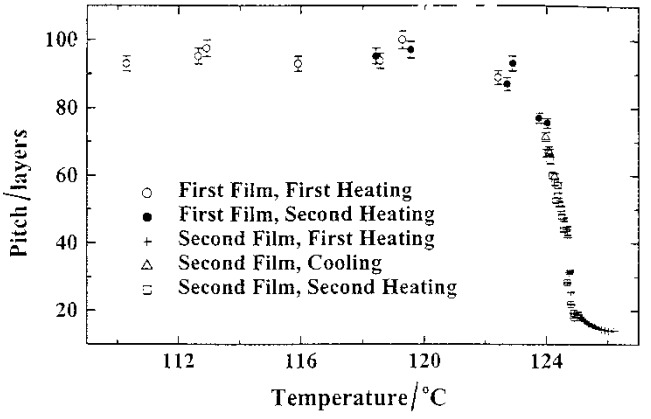

Figure 3. The measured helical pitch in smectic layers as a function of temperature obtained from 11OTBBB1M7 films. The legend labels the data collected from two films on heating and cooling. The error bars at the higher temperature are approximately the size of the symbols. The lower SmC_α*–SmC* transition temperature (124.6°C) shown here, in comparison with that from the heat capacity measurement, is due to a combination of a different synthetic batch of samples and different thermometry being used in each measurement.

which was confirmed subsequently by high resolution thermal studies.

According to an analysis of the tensor X-ray structure factor associated with a helical interlayer variation of the molecular tilt direction [22], there should exist four satellite peaks ($m=\pm1$ and ±2) around each principal Bragg peak associated with the smectic layer structure. Among the SmC* variant phases, the SmC_α* phase occurs at the highest temperature. The thermal fluctuations associated with the one-dimensional density wave, as well as the position of the heavy atom, will significantly reduce the intensity of $m=\pm2$ satellite peaks [22]. So far, only the $m=\pm1$ peaks have been unambiguously reported for a SmC_α* phase [7]. During one of the recent RXD runs, we have also confirmed the existence of the $m=2$ satellite peak in the SmC_α* phase from a 50%–50% mixture of the 10- and 11-OTBBB1M7 compounds. The data are shown in figure 4.

Although RXD is a powerful probe for measuring the incommensurate short helical pitches in both SmC_α* and SmC* phases, it requires liquid crystal compounds having one heavy element in the core of the molecule. To overcome this constraint, we have developed a complementary approach [12], employing differential optical reflectivity (DOR) [23] and null-transmission ellipsometry (NTE) [24–26], to measure the temperature evolution of the short helical pitch.

3. Differential optical reflectivity studies

As our RXD data show, in 11OTBBB1M7 the incommensurate short helical pitch is less than 30 layers in the SmC_α* phase and less than 100 layers in the SmC* phase. Thus a bulk sample in the SmC_α* phase should appear optically uniaxial. This is the main reason that the initial structural identification of the SmC_α* phase from bulk samples was inconclusive [4].

In the case of the FSF, a very different picture emerges. Due to the surface-enhanced order, surface layers of a FSF tend to have higher order than the interior layers. For example, in the SmC_α* temperature range, while the interior layers have a short helical pitch, the surface layers have the same ϕ in adjacent layers (synclinic) or opposite ϕ in adjacent layers (anticlinic) depending on the compound studied. Here ϕ denotes the azimuthal angle of the molecular tilt. Usually there exists a net polarization in the film due to the surface layers or an incomplete pitch, which allows the FSFs to be aligned by a small electric field. As the biaxial surfaces are linked to the INHP in the interior of the FSFs, DOR is sensitive to changes in the helical pitch through the biaxial surfaces.

As with the other polarization-analysed optical techniques, DOR measures the sample's effect on the

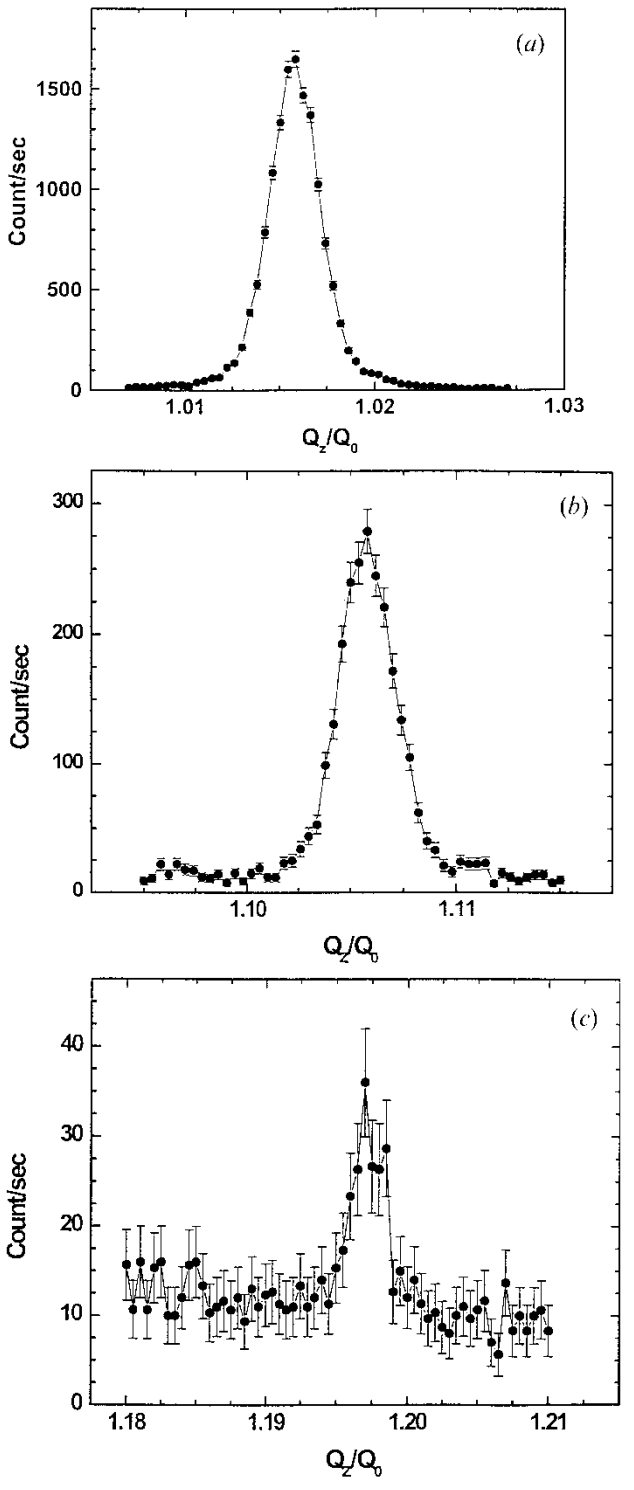

Figure 4. Resonant X-ray diffraction peaks obtained in the SmC_α* phase of a 10OTBBB1M7 (50%)–11OTBBB1M7 (50%) mixture. In these scans, Q_o was fixed so $Q_z/Q_o = 1.0$ in the uniaxial SmA phase. (*a*), (*b*) and (*c*) show, respectively; the $l=1$, $m=0$ Bragg peak, the $l=1$, $m=1$ first order satellite peak, and the $l=1$, $m=2$ second order satellite peak. The peak positions are at $Q_z = 1.0158\ Q_o$ ($m=0$), $1.1058\ Q_o$ ($m=1$) and $1.1970\ Q_o$ ($m=2$).

polarization of light. In our DOR set-up, incident 6328 Å He-Ne laser light was polarized by a Glan–Thompson polarizer mounted on a rotatable stage. After reflection off the FSF, the light was divided by a polarizing beam splitter into p- and s-polarization states, where p and s denote polarization parallel and perpendicular to the incident plane, respectively. The acquired signals were the difference, $I_p - I_s$, and the sum $I_p + I_s$, of the intensities. The experiment began with the film in the uniaxial SmA phase. At this temperature, the Glan–Thompson polarizer was rotated to yield $I_p - I_s = 0$, a condition that maximizes sensitivity to changes in the optical properties of the FSF. Upon cooling and heating the film through the SmC_α*–SmC* temperature range, we recorded $I_p - I_s$ and $I_p + I_s$ with typical temperature ramps of 10–100 mK min^{-1}. A small electric field ($E = 3\ V\,cm^{-1}$) was applied in the plane of the film to align the net polarization of the film.

Seven 11OHFBBB1M7 films ranging from 42 to 128 layers in thickness were studied [12]. A typical set of $I_p - I_s$ data obtained from a cooling run on a 97-layer film is shown in figure 5; the cooling rate was at 80 mK min^{-1}. The film was prepared over a 7 mm diameter circular hole with two parallel electrodes which allowed us to apply an electric field in the film plane, either in the same ($\alpha = 0°$) or opposite ($\alpha = 180°$)

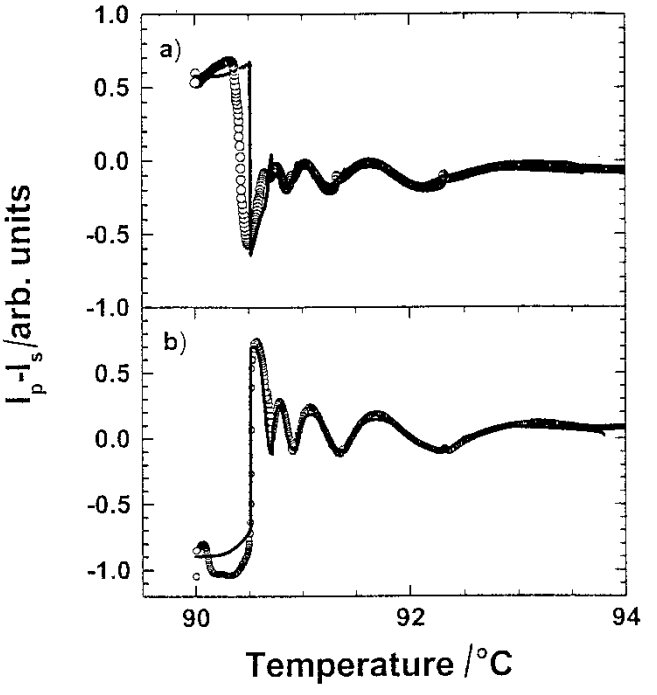

Figure 5. $I_p - I_s$ data (open circles) versus temperature obtained from a 97-layer 11OHFBBB1M7 film. The cooling rate was at 80 mK min^{-1}. The strength of the applied electric field was $3\ V\,cm^{-1}$ with $\alpha = 180°$ (*a*) and $\alpha = 0°$ (*b*). The solid lines are from simulation results.

direction as the incident laser beam direction. The strength of the electric field was $2\,V\,cm^{-1}$. The oscillatory behaviour of $I_p - I_s$ versus temperature is a characteristic of the SmC_α* phase, indicative of a temperature variation of the helical pitch [10–13]. On decreasing the temperature, the increase in the oscillating frequency with temperature shows the fast temperature variation of the helical pitch near the SmC_α*–SmC* transition as observed in the RXD results from 11OTBBB1M7 (see figure 3).

The number of surface layers, N_s, is determined by plotting the number of oscillations versus film thickness in layer number, N. The finite intercept ($N=6$) at the abscissa yields the *total* number of the surface layers. This implies that, at each surface, $N_s=3$. Employing NTE measurements from many different film thicknesses in the high temperature SmA phase, we acquired the following important parameters: the layer spacing $d=39.6\pm0.1$ Å, the ordinary index of refraction $n_o=1.467\pm0.005$, and the extraordinary index of refraction $n_e=1.595\pm0.01$. Moreover, fitting the NTE data acquired in the SmC* phase by the 4×4 matrix method [27, 28] allows us to determine the magnitude of the helical pitch. Utilizing all this information, we applied the 4×4 matrix technique to simulate the $I_p - I_s$ data. The simulation results are shown as solid lines in figure 5. The best fit yields the temperature variation of pitch as shown in figure 6. As with the results on 11OTBBB1M7, in the SmC* phase, the magnitude of the pitch is about 70 layers; while in the SmC_α* phase, the magnitude of the pitch is approximately 15 layers. In the neighbourhood of the phase transition, there exists a fast variation of the helical pitch. Within our resolution, we detected no jump at the transition temperature nor any thermal hysteresis between the successive heating and cooling runs.

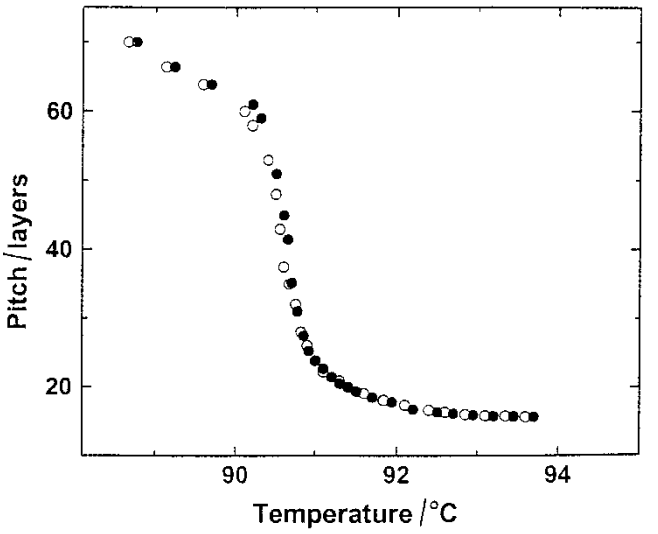

Figure 6. The temperature variation of the pitch used to simulate the experimental data shown in figure 5. The orientation of the electric field $\alpha=180^\circ$ (open circles) and $\alpha=0^\circ$ (solid dots). The lower SmC_α*–SmC* transition temperature (90.5°C) shown here, in comparison with that from the heat capacity measurement, is due to a combination of a different synthetic batch of samples and different thermometry being used in each measurement.

4. Calorimetric investigations

Heat capacity has been measured with a high resolution calorimeter, which can be operated in an ultra-low frequency (0.03125 Hz in the standard operation) a.c. mode [29] as well as in a non-adiabatic scanning (NAS) mode [30]. Hermetically sealed gold cells that contained about 10–30 mg of liquid crystal sample were used. The temperature scan rate was about $0.03\,K\,h^{-1}$ in the transition region. Very slow drift rates in the SmA–SmC_α*–SmC* transition temperatures, about -10 mK per day, indicate the stability and high quality of the sample (to help the comparison between the data of successive runs, the temperature scale has been adjusted so that the transition temperatures agree with those obtained just after the cell was prepared). The C_p values were determined from the following expression:

$$C_p = \left(C_{p,\,\mathrm{obs}} - C_{p,\,\mathrm{empty}}\right)/m.$$

Here $C_{p,\mathrm{obs}}$ and $C_{p,\mathrm{empty}}$ are the heat capacity of the filled and empty cells, respectively, and m is the mass of the liquid crystal sample in grams.

The C_p data for 11OHFBBB1M7 obtained in the a.c. mode are displayed in figure 7. In the neighbourhood of the SmA–SmC_α* transition, the heat capacity displays a lamda-shape. In contrast, as shown in the inset, a very

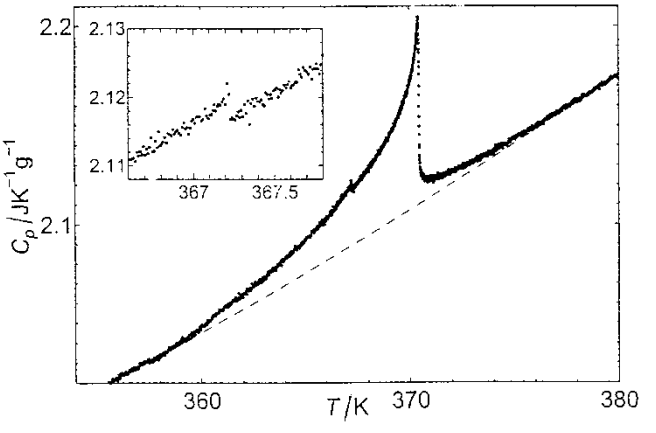

Figure 7. Temperature dependence of the heat capacity C_p of 11OHFBBB1M7 obtained in the a.c. mode measurement. Dashed line shows a background heat capacity.

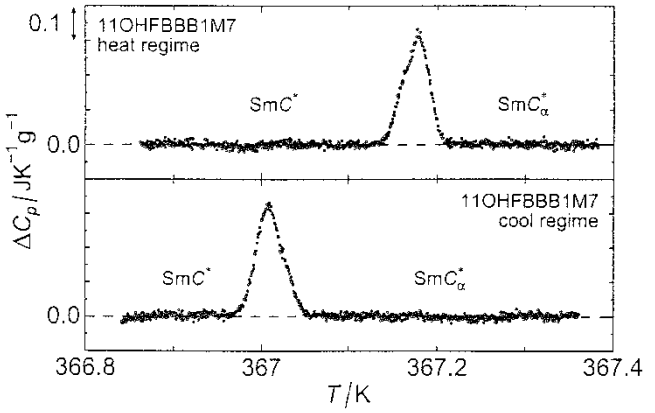

Figure 8. Temperature dependence of the excess heat capacity ΔC_p of 11OHFBBB1M7 near the SmC_α*–SmC* transition obtained in NAS mode measurement during heating and cooling runs.

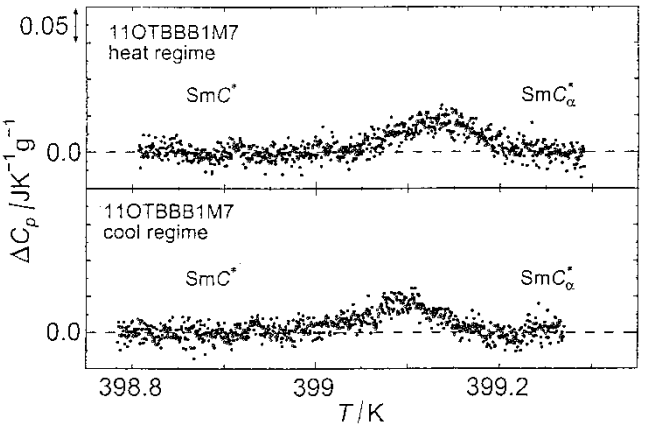

Figure 10. Temperature dependence of the excess heat capacity ΔC_p of 11OTBBB1M7 near the SmC_α*–SmC* transition obtained in NAS mode measurement during heating and cooling runs.

small heat capacity step is discernible at the SmC_α*–SmC* transition. Figure 8 depicts the data near this SmC_α*–SmC* transition obtained in the NAS mode. Heat (cool) regime data correspond to data obtained during an NAS heating (cooling) scan, respectively. A clear peak, with a very narrow temperature width of about 0.08 K and a thermal hysteresis of about 0.18 K, is discernible. By interpreting this peak in the NAS data as latent heat, we conclude that the transition is first order. Integration of the NAS peak yielded a latent heat of 7–8 $J\,mol^{-1}$, which agrees with the value 8 $J\,mol^{-1}$ obtained by a DSC measurement [31].

The data for 11OTBBB1M7 acquired in the a.c. mode are shown in figure 9. The heat capacity behaviour at the SmA–SmC_α* transition is similar to that from 11OHFBBB1M7; however, a broad hump-like feature is seen near the SmC_α*–SmC* transition of 11OTBBB1M7. Figure 10 displays the data near the SmC_α*–SmC* transition obtained in the NAS mode. The feature has a temperature width of about 0.2 K and a thermal hysteresis of approximately 0.05 K or less. Although this feature is rather broad, a simple and probable explanation is to ascribe it to latent heat.

A question arises, then, about the relation between the broad features observed in both the NAS and a.c. mode measurements. It is well known that to detect latent heat in the a.c. mode is a difficult task [32]. The height and width of the humps obtained from the a.c. and NAS modes are both considerably different. Thus, it seems unrealistic to consider that the features observed in these two modes have the same physical origin, e.g. latent heat. Further evidence that they are distinct features is the fact that the *sum* of their integrated entropy changes, 4–5 $J\,mol^{-1}$, roughly agrees with the value 6 $J\,mol^{-1}$ obtained from a DSC measurement [33]. A plausible explanation is the existence of slow relaxation processes during the transition. Further studies are needed to address this question.

To analyse the heat capacity behaviour near the SmA–SmC_α* transition, the excess heat capacity ΔC_p was calculated from

$$\Delta C_p = C_p - C_p(\text{background}).$$

Here C_p(background) is the background heat capacity, determined as a quadratic function of the temperature which joins the measured heat capacity data smoothly at temperatures away from the transition on both sides of it. In figures 7 and 9, C_p(background) is shown as dashed lines. The data have been analysed with the

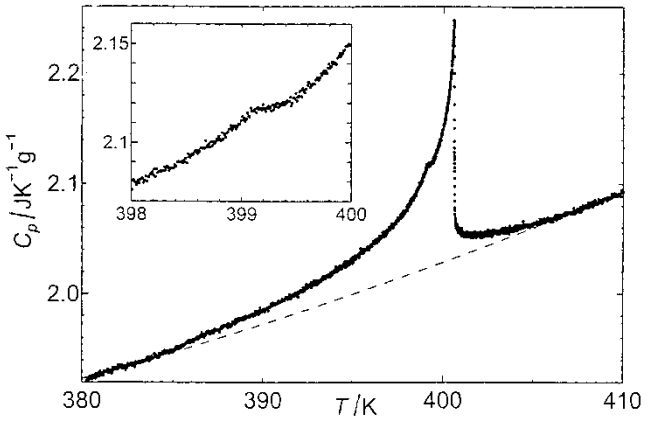

Figure 9. Temperature dependence of the heat capacity C_p of 11OTBBB1M7 acquired in a.c. mode measurement. The dashed line shows background heat capacity. The inset exhibits details of the heat capacity data near the SmC_α*–SmC* transition.

Table 1. Least-squares values of the adjustable parameters for fitting ΔC_p with equation (1). The units for A^+ and B_c are $J\,K^{-1}\,g^{-1}$.

System	$\|t\|_{max}$	T_c/K	α	$10^3\ A^+$	A^-/A^+	D_1^+	D_1^-	B_c	χ_v^2
11OHF	0.001	370.460	0.018	5.015	1.271	0.718	−1.635	−0.312	1.00
	0.003	370.460	0.054	3.147	1.915	1.318	−3.072	−0.078	1.10
	0.01	370.461	0.088	1.734	2.999	−0.193	−4.379	−0.026	1.18
11OT	0.001	400.546	0.043	6.390	1.925	1.265	−4.831	−0.186	1.00
	0.003	400.547	0.102	2.475	4.199	−2.722	−6.464	−0.025	1.11
	0.01	400.546	0.128	1.898	5.129	−6.052	−4.604	−0.011	1.05

following renormalization-group expression including correction-to-scaling terms [34]:

$$\Delta C_p = \left(A^{\pm}/\alpha\right)|t|^{-\alpha}\left(1 + D_1^{\pm}|t|^{\Delta_1} + D_2^{\pm}|t|\right) + B_c. \quad (1)$$

Here $t = (T - T_c)/T_c$ and the superscripts $\pm$ denote above and below T_c. To avoid an extraneous contribution from the SmC_α*–SmC* transition, the data in the range 366.70–367.22 K for 11OHFBBB1M7 and 398.19–399.33 K for 11OTBBB1M7, were omitted from the fit. Although the correction-to-scaling exponent Δ_1 is dependent on the universality class, its theoretically predicted values are close to 0.5 [34, 35]. Therefore, its value was fixed at 0.5 in these fits. The second order correction coefficients $D_2^{\pm}$ were fixed at zero. Fits were made to the data over several ranges, and the maximum value of $|t|$ used in the fit, denoted as t_{max}, is shown in the table. Table 1 summarizes the values of the critical exponent α and the remaining adjustable parameters thus obtained. The exponent α was unconstrained in the least-squares fitting procedure. It is seen that the value of α shows a noticeable dependence on the fitting range, suggesting a crossover behaviour such as the one observed in MHPOBC and related substances [36]. In the small t_{max} limit, α approaches the 3D XY value, $\alpha = -0.0066$ [34].

By holding the exponent fixed at the 3D XY values: $\alpha = -0.0066$ and $\Delta_1 = 0.524$ [34], we also conducted fits. The parameter values are shown in table 2. Both cases of fixing $D_2^{\pm} = 0$ and allowing $D_2^{\pm}$ to have non-zero values have been tried. Using different T_c values for different data ranges is inconsistent, and is likely to give artificially good fits. To avoid this, we fixed T_c to the value determined in the narrowest data range. When the second order correction terms are neglected ($D_2^{\pm} = 0$), the fit over the data range $t_{max} = 0.001$ is sufficiently good in the χ_v^2 sense, while the fits become worse for larger t_{max}. Inclusion of the second order correction term improves χ_v^2 adequately. In figures 11 and 12, the solid lines are fitting curves with parameter values listed in the last rows for each system in table 2. A violation of the scaling prediction $D_1^+ = D_1^-$ is seen irrespective of fixing $D_2^{\pm}$ to have non-zero values. ($D_1^+ = D_1^-$ is expected in the ε-expansion calculation to the leading order in ε [37]; the values of D_1^+/D_1^- obtained in the ε-expansion up to higher order and in the field theory are only slightly larger than unity for 3D XY universality class: 1.17 and 1.6, respectively [38].) Such a tendency is similar to the case of MHPOBC-group substances [36], and might be an indication of the crossover. As another remarkable trend, the critical amplitude ratio A^-/A^+ is not far from, but substantially smaller than the theoretical values for the 3D XY model, $A^-/A^+ = 0.971 \pm 0.013$ [34]. This situation

Table 2. Least-squares values of the adjustable parameters for fitting ΔC_p with equation (1). In these fits, the exponent values were fixed to 3D XY values, $\alpha = -0.0066$, and $\Delta_1 = 0.524$. Quantities in brackets were held fixed at the given values. The units for A^+ and B_c are $J\,K^{-1}\,g^{-1}$.

System	$\|t\|_{max}$	T_c/K	$10^3\ A^+$	A^-/A^+	D_1^+	D_1^-	D_2^+	D_2^-	B_c	χ_v^2
11OHF	0.001	370.460	6.552	0.905	−0.325	1.063	[0]	[0]	0.951	1.04
	0.003	[370.460]	6.519	0.910	−0.251	0.841	[0]	[0]	0.947	1.89
	0.01	[370.460]	6.520	0.918	−0.151	0.622	[0]	[0]	0.950	5.56
	0.003	[370.460]	6.989	0.908	−0.489	1.239	3.06	−6.42	1.012	1.10
	0.01	[370.460]	6.500	0.905	−0.363	1.187	1.72	4.58	0.944	1.14
11OT	0.001	400.540	16.012	0.913	−0.430	1.046	[0]	[0]	2.313	1.21
	0.003	[400.540]	15.629	0.918	−0.278	0.830	[0]	[0]	2.264	3.41
	0.01	[400.540]	16.130	0.929	−0.174	0.524	[0]	[0]	2.342	9.74
	0.003	[400.540]	15.517	0.906	−0.589	1.646	4.41	−10.72	2.241	0.97
	0.01	[400.460]	14.672	0.907	−0.393	1.396	1.97	−6.30	2.124	1.31

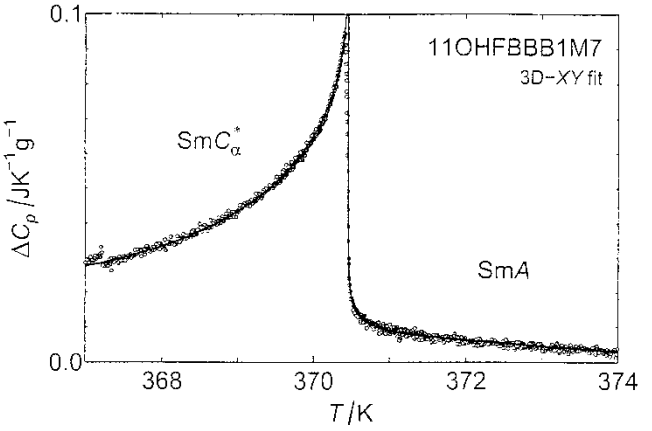

Figure 11. Temperature variation of the excess heat capacity ΔC_p of 11OHFBBB1M7 in the vicinity of the SmA–SmC$_\alpha$* transition. The solid line is the fit of the data with equation (1).

can be compared to other 3D *XY* systems. In MHPOBC-group substances, the ratio is closer to the theoretical value, being 0.930–0.957 [33]. For the N–SmA transition, on the other hand, the ratio is slightly larger than the theoretical value, being 0.983–0.994 [39].

To summarize, the previously measured tendency of the SmA–SmC$_\alpha$* transition to exhibit 3D *XY* behaviour, which crosses over to a tricritical one, has been strengthened by new measurements on 11OHFBBB1M7 and 11OTBBB1M7. Moreover, although the critical amplitude ratio A^-/A^+ is predicted to be a universal constant, significant variation was observed. This latter point is quite puzzling and should be investigated further.

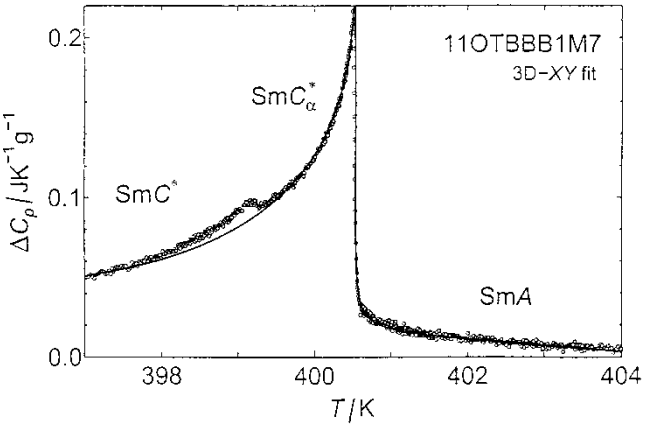

Figure 12. Temperature dependence of the excess heat capacity ΔC_p of 11OTBBB1M7 near the SmA–SmC$_\alpha$* transition. The solid line is the fit of the data with equation (1).

5. Discussion

In the neighbourhood of theSmC$_\alpha$*–SmC* transition, the measured helical pitch shows a rapid variation with temperature. Thermal studies clearly show that they are weakly first order transitions. Thus, our results indicate that both compounds should not be too far from their critical points associated with the SmC$_\alpha$*–SmC* transition. In principle, such a critical point should be accessible by appropriate binary mixtures. Experimentally, it would be extremely important to conduct detailed investigations of the nature of this critical point.

The SmA–SmC* transition is characterized by at least three distinct physical quantities: tilt angle, polarization, and helical pitch. They are zero in the SmA phase and have finite values in the SmC* phase. Experimentally, it is well established that the parameter $\theta \exp(i\phi)$, describing the molecular tilt from the layer normal, is the principal order parameter associated with the SmA–SmC* transitions. Here θ is the magnitude of the tilt angle and ϕ the azimuthal angle indicating the in-plane tilt direction. Similarly, to the best of our knowledge the tilt angle is also the principal order parameter associated with the SmA–SmC$_\alpha$* transition. Thus, both the SmA–SmC* and the SmA–SmC$_\alpha$* transitions belong to the *XY*-universality class and should show the same critical phenomena.

From high resolution heat capacity measurements, Huang and Viner [40] were able to understand the behaviour of the SmA–SmC (or SmC*) transitions in the context of an extended mean-field model. To date, it remains a puzzle that the conventional SmA–SmC (or SmC*) transitions show a large correlation length [41] and can be described by mean-field behaviour. In recent years, Ema and Yao [36] have conducted high resolution heat capacity studies on several compounds, possessing a 1-methylheptyl chiral tail and exhibiting the SmA–SmC$_\alpha$* transition. Their heat capacity data can be described by either the *XY*-model or a crossover between the *XY* and the Gaussian tricritical models. Experimentally it is well established that the INHP found in the SmC$_\alpha$* phase is a result of frustration between n.n. ferroelectric and n.n.n. antiferroelectric interactions. Consequently, the molecular tilt angle found in this class of liquid crystal compounds can also be due to such short range molecular interactions (n.n. and n.n.n.) Potentially, this scenario could explain the observed *XY*-like behaviour observed for the SmA–SmC$_\alpha$* transition. Thermal studies on compounds possessing a 1-methylheptyl chiral tail and exhibiting a *direct* SmA–SmC* transition should further elucidate this hypothesis.

This work was partially supported by the National Science Foundation under Grants No. DMR-0106122

and INT-9815859, and Grant-in-Aid for Scientific Research by the Ministry of Education and Science, No. 12129204. The research was carried out in part at the National Synchrotron Light Source, Brookhaven National Laboratory, which is supported by the U.S. Department of Energy, Division of Materials Sciences and Division of Chemical Sciences, under Contract No. DE-AC02-98CH10886.

References

[1] Chandani, A. D. L., Gorecka, E., Ouchi, Y., Takezoe, H., and Fukuda, A., 1989, *Jpn. J. appl. Phys.*, **28,** L1265.
[2] Chandani, A. D. L., Ouchi, Y., Takezoe, H., Fukuda, A., Terashima, K., Furukawa, K., and Kishi, A., 1989, *Jpn. J. appl. Phys.*, **28,** L1261.
[3] Gorecka, E., Chandani, A. D. L., Ouchi, Y., Takezoe, H., and Fukuda, A., 1990, *Jpn. J. appl. Phys.*, **29,** 131.
[4] Takanishi, Y., Ikeda, A., Takezoe, H., and Fukuda, A., 1995, *Phys. Rev. E*, **51,** 400.
[5] Matsumoto, T., Fukuda, A., Johno, M., Motoyama, Y., Yui, T., Seomun, S., and Yamashita, M., 1999, *J. mater. Chem.*, **9,** 2051.
[6] Fukuda, A., Takanishi, Y., Isozaki, T., Ishikawa, K., and Takezoe, H., 1994, *J. mater. Chem.*, **4,** 997.
[7] Mach, P., Pindak, R., Levelut, A.-M., Barois, P., Nguyen, H. T., Huang, C. C., and Furenlid, L., 1998, *Phys. Rev. Lett.*, **81,** 1015.
[8] Mach, P., Pindak, R., Levelut, A.-M., Barois, P., Nguyen, H. T., Baltes, H., Hird, M., Toyne, K., Seed, A., Goodby, J. W., Huang, C. C., and Furenlid, L., 1999, *Phys. Rev. E*, **60,** 6793.
[9] Cady, A., Pitney, J. A., Pindak, R., Matkin, L. S., Watson, S. J., Gleeson, H. F., Cluzeau, P., Barois, P., Levelut, A.-M., Caliebe, W., Goodby, J. W., Hird, M., and Huang, C. C., 2001, *Phys. Rev. E*, **64,** 050702.
[10] Johnson, P. M., Pankratz, S., Mach, P., Nguyen, H. T., and Huang, C. C., 1999, *Phys. Rev. Lett.*, **83,** 4073.
[11] Olson, D. A., Pankratz, S., Johnson, P. M., Cady, A., Nguyen, H. T., and Huang, C. C., 2001, *Phys. Rev. E*, **63,** 061711.
[12] Cady, A., Olson, D. A., Han, X. F., Nguyen, H. T., and Huang, C. C., 2002, *Phys. Rev. E*, **65,** 030701.
[13] Schlauf, D., Bahr, CH., and Nguyen, H. T., 1999, *Phys. Rev. E*, **60,** 6816.
[14] Hirst, L. S., Watson, S. J., Gleeson, H. F., Cluzeau, P., Barois, P., Pindak, R., Pitney, J., Cady, A., Johnson, P. M., Huang, C. C., Levelut, A-M., Srajer, G., Pollmann, J., Caliebe, W., Seed, A., Herbert, M. R., Goodby, J. W., and Hird, M., 2002, *Phys. Rev. E*, **65,** 041705.
[15] Yamashita, M., 1996, *J. phys. Soc. Jpn.*, **65,** 2904; Yamashita M., 1998, *J. phys. Soc. Jpn.*, **67,** 198.
[16] Cepic, M., and Zeks, B., 1995, *Mol. Cryst. liq. Cryst.*, **263,** 61; Cepic, M., and Zeks, B., 2001, *Phys. Rev. Lett.*, **87,** 85501.
[17] Lorman, V. L., 1995, *Mol. Cryst. liq. Cryst.*, **262,** 437.
[18] Roy, A., and Madhusudana, N. V., 1996, *Europhys. Lett.*, **36,** 221.
[19] Pikin, S., Gorkunov, M., Kilian, D., and Haase, W., 1999, *Liq. Cryst.*, **26,** 1107.
[20] Osipov, M. A., and Fukuda, A., 2000, *Phys. Rev. E*, **62,** 3724.
[21] Olson, D. A., Han, X. F., Cady, A., and Huang, C. C., 2002, *Phys. Rev. E*, **66,** 021 702.
[22] Levelut, A.-M., and Pansu, B., 1999, *Phys. Rev. E*, **60,** 6803.
[23] Pankratz, S., Johnson, P. M., and Huang, C. C., 2000, *Rev. Sci. Instrum.*, **71,** 3184.
[24] Azzam, R. M. A., and Bashara, N. M., 1989, *Ellipsometry and Polarized Light* (Amsterdam: North-Holland).
[25] Bahr, Ch., and Fliegner, D., 1992, *Phys. Rev. A*, **46,** 7657.
[26] Olson, D. A., Han, X. F., Johnson, P. M., Cady, A., and Huang, C. C., 2002, *Liq. Cryst.*, **29,** 1521.
[27] Berreman, D. W., 1972, *J. opt. Soc. Am.*, **62,** 502.
[28] Wohler, H., Haas, G., Fritsch, M., and Mlynski, D. A., 1988, *J. opt. Soc. Am. A*, **5,** 1554.
[29] Ema, K., and Yao, H., 1997, *Thermochim. Acta*, **304/305,** 157.
[30] Yao, H., Ema, K., and Garland, C. W., 1998, *Rev. sci. Instrum*, **69,** 172.
[31] Faye, V., Rouillon, J. C., and Destrade, C., 1995, *Liq. Cryst.*, **19,** 47.
[32] Kutnjak, Z., Garland, C. W., Shatz, C. G., Collings, P. J., Booth, C. J., and Goodby, J. W., 1996, *Phys. Rev. E*, **53,** 4955.
[33] Nguyen, H. T., Rouillon, J. C., Cluzeau, P., Sigaud, G., Destrade, V. C., and Isaert, N., 1994, *Liq. Cryst.*, **17,** 571.
[34] Bagnuls, C., and Bervillier, C., 1985, *Phys. Rev. B*, **32,** 7209; Bervillier C., 1986, *Phys. Rev. B*, **34,** 8141; Bagnuls, C., Bervillier, C., Meiron, D. I., and Nickel, B. G., 1987, *Phys. Rev. B*, **35,** 3583.
[35] Zinn, S. Y., and Fisher, M. E., 1996, *Physica*, **226,** 168.
[36] Ema, K., and Yao, H., 1998, *Phys. Rev. E*, **57,** 6677.
[37] Aharony, A., and Ahlers, G., 1980, *Phys. Rev. Lett.*, **44,** 782.
[38] Privman, V., Hohenberg, P. C., and Aharony, A., 1991, in *Phase Transitions and Critical Phenomena*, Vol. 14, edited by C. Dome, and J. L. Lebowitz (New York: Academic).
[39] Garland, C. W., Nounesis, G., Young, M. J., and Birgeneau, R. J., 1993, *Phys. Rev. E*, **47,** 1918.
[40] Huang, C. C., and Viner, J. M., 1982, *Phys. Rev. A*, **25,** 3385.
[41] Safinya, C. R., Kaplan, M., Als-Nielsen, J., Birgeneau, R. J., Davidov, D., Litster, J. D., Johnson, D. L., and Neubert, M., 1980, *Phys. Rev. B*, **21,** 4149.